Conversion of Photoluminescence Blinking Types in Single Colloidal Quantum Dots

Changgang Yang, Yang Li, Xiaoqi Hou, Mi Zhang, Guofeng Zhang,* Bin Li, Wenli Guo, Xue Han, Xiuqing Bai, Jialu Li, Ruiyun Chen, Chengbing Qin, Jianyong Hu, Liantuan Xiao,* and Suotang Jia

Almost all colloidal quantum dots (QDs) exhibit undesired photoluminescence (PL) blinking, which poses a significant obstacle to their use in numerous luminescence applications. An in-depth study of the blinking behavior, along with the associated mechanisms, can provide critical opportunities for fabricating high-quality QDs for diverse applications. Here the blinking of a large series of colloidal QDs is investigated with different surface ligands, particle sizes, shell thicknesses, and compositions. It is found that the blinking behavior of single alloyed CdSe/ZnS QDs with a shell thickness of up to 2 nm undergoes an irreversible conversion from Auger-blinking to band-edge carrier blinking (BC-blinking). Contrastingly, single perovskite QDs with particle sizes smaller than their Bohr diameters exhibit reversible conversion between BC-blinking and more pronounced Auger-blinking. Changes in the effective trapping sites under different excitation conditions are found to be responsible for the blinking type conversions. Additionally, changes in shell thickness and particle size of QDs have a significant effect on the blinking type conversions due to altered wavefunction overlap between excitons and effective trapping sites. This study elucidates the discrepancies in the blinking behavior of various QD samples observed in previous reports and provides deeper understanding of the mechanisms underlying diverse types of blinking.

1. Introduction

Colloidal semiconductor quantum dots (QDs) that have size-dependent absorption and emission properties along with high photoluminescence (PL) quantum yields (QYs) have a wide range of applications such as light-emitting diodes, lasers, photodetectors, and solar cells.[1–4] Although there has been significant progress in the synthesis and application of QDs, undesirable PL blinking, often present in almost all colloidal QDs, continues to be a substantial obstacle when it comes to relevant applications. PL blinking is a random fluctuation of a single-QD PL intensity, and it can be identified by the step-wise switching between the bright and dim states in the PL intensity time trace.[5] Although blinking-free single-QD PL has been successfully demonstrated in pure-phase zinc-blende as well as wurtzite CdSe/CdS QD systems, this has only been achieved under very weak excitation conditions.[6,7] Furthermore, although non-blinking "Giant" core/shell QDs up to ≈50 nm in size have been successfully constructed,[8,9] the large particle size is generally not recommended for biomedical applications.[7,10,11] Their thick shell structures also impede the transport of charge carriers, making them unsuitable for photoelectric and photovoltaic applications. As a result, compact QDs are often preferred for a variety of applications, but PL blinking is inevitably present in these compact QDs, which has an impact on their associated applications.

C. Yang, M. Zhang, G. Zhang, B. Li, W. Guo, X. Han, X. Bai, J. Li, R. Chen, C. Qin, J. Hu, L. Xiao, S. Jia
State Key Laboratory of Quantum Optics and Quantum Optics Devices
Institute of Laser Spectroscopy
Collaborative Innovation Center of Extreme Optics
Shanxi University
Taiyuan 030006, China
E-mail: guofeng.zhang@sxu.edu.cn; xlt@sxu.edu.cn
Y. Li
School of Physics and Optoelectronic Engineering
Hangzhou Institute for Advanced Study
University of Chinese Academy of Sciences
Hangzhou 310024, China

Y. Li
Research Institute of Intelligent Sensing
Zhejiang Lab
Hangzhou 311100, China
X. Hou
School of Chemistry and Material Science
Hangzhou Institute for Advanced Study
University of Chinese Academy of Sciences
Hangzhou 310024, China

**ADVANCED
SCIENCE NEWS**

www.advancedsciencenews.com

NANO · MICRO

small

www.small-journal.com

Therefore, an in-depth study of the blinking behavior is crucial for the design of compact, blinking-free QDs suitable for various applications.

The pioneering works explain PL blinking separately according to the charging model and the multiple recombination centers (MRC) model.[5,12,13] The charging model attributes the PL blinking to the random photoionization and neutralization.[5,12] Radiative recombination of a single exciton in a neutral QD produces the bright state of a PL intensity trajectory. Non-radiative Auger recombination is triggered when the QD is photoionized, causing the exciton recombination energy to transfer to the extra charge carrier and quenching the PL emission. Facilitated by non-radiative Auger recombination, this blinking behavior is also known as Auger-blinking.[14] It is noteworthy that Auger-blinking requires a long-lived trap that can capture one photoexcited carrier for a long time to allow the creation of a second exciton and the formation of a trion state.[14–18] Nevertheless, the charging model is incapable of accounting for the other type of blinking behavior that manifests itself as continuous emission states with varying non-radiative rates and fixed radiative rates.[19–21] The MRC model was proposed to account for this blinking behavior, other than Auger-blinking.[13] The MRC model suggests that the activation and deactivation of a set of non-radiative recombination centers modifies the non-radiative rate of single excitons, thereby modulating the PL intensity. The non-radiative recombination centers are regarded as short-lived traps for band-edge carriers.[14] Since this blinking arises from the trapping of band-edge carriers, this blinking behavior is termed as BC-blinking.

The charging model and the MRC model describe different correlations between the PL intensity and the PL lifetime in distinct mechanisms. Thus, fluorescence lifetime-intensity distribution (FLID) maps have been effective in identifying the PL blinking types of single QDs.[13,14,22,23] Auger blinking results in a non-linear (curved) FLID map. On the other hand, BC-blinking results in a linear FLID map.[14,19,22] From the FLID maps, all the two types of blinking could be observed in CdSe-based QDs and perovskite QDs.[5,12,14,15,22–31] Furthermore, two different blinking types could coexist in CdSe-based QDs and perovskite QDs.[14,32–34] The rich variety in the reported observations raises some fundamental questions: why do the QDs with the same chemical compositions and from the same production batch exhibit distinct blinking types? can the blinking type of QDs be converted during the PL emission process, and what is the driving factor behind such conversions?

In the work, we investigate the PL blinking behavior of alloyed CdSe/ZnS QDs with different surface ligands, particle sizes and shell thicknesses, as well as perovskite QDs with different particle sizes and compositions using single-dot PL spectroscopy. It is found that the blinking type of some QD can be changed by tuning the laser pump fluence during the PL emission process. For single alloyed CdSe/ZnS QDs with a shell thickness of up to 2 nm, when the laser pump fluence increases to a specific threshold, PL blinking type can convert irreversibly from Auger-blinking to BC-blinking. Intriguingly, for single perovskite QDs with particle sizes smaller than their Bohr diameters, the PL blinking type can be reversibly converted from BC-blinking to a more pronounced Auger-blinking by increasing or decreasing the laser fluence. By analyzing these blinking type conversion processes, it is found that changes in effective trapping sites under different excitation conditions are responsible for the conversion of PL blinking types. This investigation provides an explanation for the discrepancies found in previous literature reports and can provide greater insight into the mechanisms behind the different types of blinking under various excitation conditions.

2. Results and Discussion

2.1. Blinking Type of Single Colloidal QDs under Weak Excitation Conditions

We first identify the blinking types of single colloidal QDs under weak excitation conditions, using alloyed CdSe/ZnS QDs with a shell thickness of ≈2.0 nm and $CH_3NH_3PbBr_3$ perovskite QDs with a particle size of ≈3.2 nm as examples. The excitation condition for single QD studies is generally represented by the average number of photons absorbed per QD per pulse, $<N>$. When the $<N>$ value is less than 0.3, it is considered to be a weak excitation condition.[35,36] The method of estimating the $<N>$ value can be based on previous work.[30,32,37,38] The synthesis methods of alloyed CdSe/ZnS QDs and $CH_3NH_3PbBr_3$ perovskite QDs can be found in METHODS. Transmission electron microscopy images of alloyed CdSe/ZnS QDs and perovskite QDs are shown in **Figure 1a,b**. The diameter of alloyed CdSe/ZnS core/shell QDs is ≈12.2 nm, and the ZnS shell thickness is ≈2.0 nm. The size of $CH_3NH_3PbBr_3$ perovskite QDs is ≈3.2 nm. The absorption and PL spectra of the alloyed CdSe/ZnS QDs and $CH_3NH_3PbBr_3$ perovskite QDs, and the elemental distribution maps of the alloyed CdSe/ZnS QDs are shown in Figures S1 and S2 (Supporting Information). The elemental distribution of the CdSe/ZnS QDs shows that the core contains Zn elements and the shell contains Cd elements, indicating that the QDs are alloyed, as detailed in the METHOD.

A typical PL blinking trajectory of single alloyed CdSe/ZnS QDs with a bin time of 10 ms at $<N> = 0.1$ and the corresponding FLID map are shown in Figure 1c. The FLID map is constructed using the same method as described in the literature,[22,23] where the lifetime value is averaged from the arrival time of each bin's PL photons. The PL trajectory displays two intensity regions at 760 Counts/10 ms (I_1, red dotted line) and 280 Counts/10 ms (I_2, black dotted line), which correspond to the PL lifetime values of 24.7 ns (τ_1) and 5.0 (τ_2) ns, respectively. The PL lifetime values are obtained by employing exponential functions to fit the PL decay curves extracted from the two intensity regions (Figure S4, Supporting Information). Based on these PL intensity and lifetime values, we could calculate the ratio of radiative rates ($\beta = I_2\tau_1/I_1\tau_2$) between the two PL regions to be ≈2, indicating that the two PL regions are neutral exciton (red) and trion (black) states, respectively.[39] Although the different emission states in PL intensity trajectory can be effectively distinguished by calculating the ratio of the radiative rates, the use of FLID maps can provide a more intuitive and comprehensive insight into the blinking mechanisms involved in QDs. The typical FLID map of alloyed CdSe/ZnS QDs under weak excitation conditions is shown in the right panel of Figure 1c, which shows a non-linear distribution. To simulate this FLID map, we initially assume that the observed

**ADVANCED
SCIENCE NEWS**

www.advancedsciencenews.com

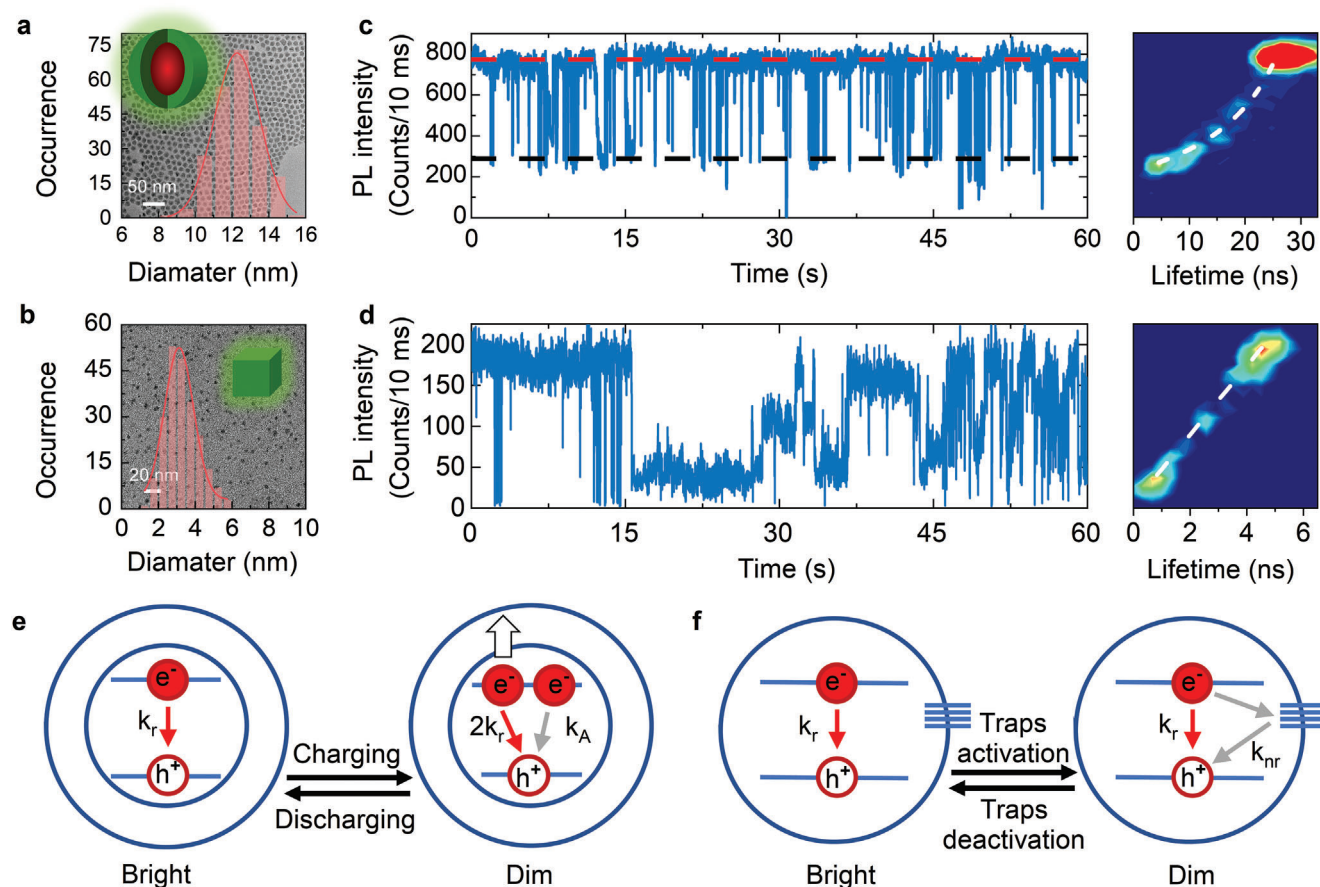NANO · MICRO

small

www.small-journal.com

Figure 1. Auger-blinking and band-edge carrier blinking (BC-blinking) of colloidal quantum dots (QDs). a,b) Transmission electron microscopy images and size distributions for alloyed CdSe/ZnS QDs and $CH_3NH_3PbBr_3$ perovskite QDs, respectively. c) Typical Photoluminescence (PL) blinking trajectory of single alloyed CdSe/ZnS QDs at excitation condition $<N> = 0.1$ and corresponding fluorescence intensity-lifetime distribution (FLID) map. The white dotted line in the FLID map is the simulated lines, given by Equation 1. d) Typical PL blinking trajectory of single $CH_3NH_3PbBr_3$ perovskite QDs at $<N> = 0.1$ and corresponding FLID map. The white dotted line in the FLID map is given by Equation 2. e) Schematic of Auger-blinking mechanism. f) Schematic of BC-blinking mechanism.

blinking results from switching between the neutral exciton and trion states. Therefore, the intermediate state or transition between neutral exciton and trion states in the PL intensity trajectory may be considered a mixture of neutral exciton and trion emissions. Within a time bin of T, we could assume that a single QD stays in the neutral exciton state (intensity I_1 and lifetime τ_1) for time T_1, and stays in the trion state (intensity I_2 and lifetime τ_2) for time T_2, and $T = T_1 + T_2$. The average PL intensity I and the average lifetime τ per bin time T can be represented by $I = \frac{I_1 T_1 + I_2 T_2}{T}$ and $\tau = \frac{I_1 T_1 \tau_1 + I_2 T_2 \tau_2}{I_1 T_1 + I_2 T_2}$, respectively. Thus, the average PL intensity I is inversely proportional to the average lifetime τ as:[14]

$$I = \frac{I_1 I_2 (\tau_2 - \tau_1)}{I_2 (\tau_2 - \tau) + I_1 (-\tau_1 + \tau)} \tag{1}$$

The curved FLID map in the right panel of Figure 1c can be well simulated by Equation 1, as shown by the white dotted line. This good simulation indicates that the observed PL blinking is a pure Auger-blinking. The Auger-blinking originates from the exciton-trion transitions, as schematically described in Figure 1e.

On the one hand, the radiative recombination comes from the single exciton state, and k_r is the radiative rate (left panel of Figure 1e). On the other hand, when a QD is charged (an extra charge is introduced into the QD), the single exciton state is transformed into a trion state. The radiative rate of the trion state becomes twice the radiative rate of the single exciton state, due to the twofold increase in the number of recombination channels (right panel of Figure 1e).[17,40,41] Although the trion state has a radiative rate of $2k_r$, the non-radiative Auger recombination of the trion state is stronger than its radiative recombination, and thus is able to strongly quench the PL intensity of the QD. It is worth mentioning that all the QDs investigated in this study have been confirmed to be single QDs by the second-order correlation function ($g^{(2)}$) method (Figure S5, Supporting Information), and the low $g^2(0)$ value in each figure indicates that the observed PL originates from a single QD.

Figure 1d shows a typical PL blinking trajectory of single $CH_3NH_3PbBr_3$ perovskite QDs at $<N> = 0.1$, along with the corresponding FLID map. As the FLID map looks like a linear correlation between the PL intensity and the PL lifetime, we infer that the observed PL blinking is BC-blinking. According to the
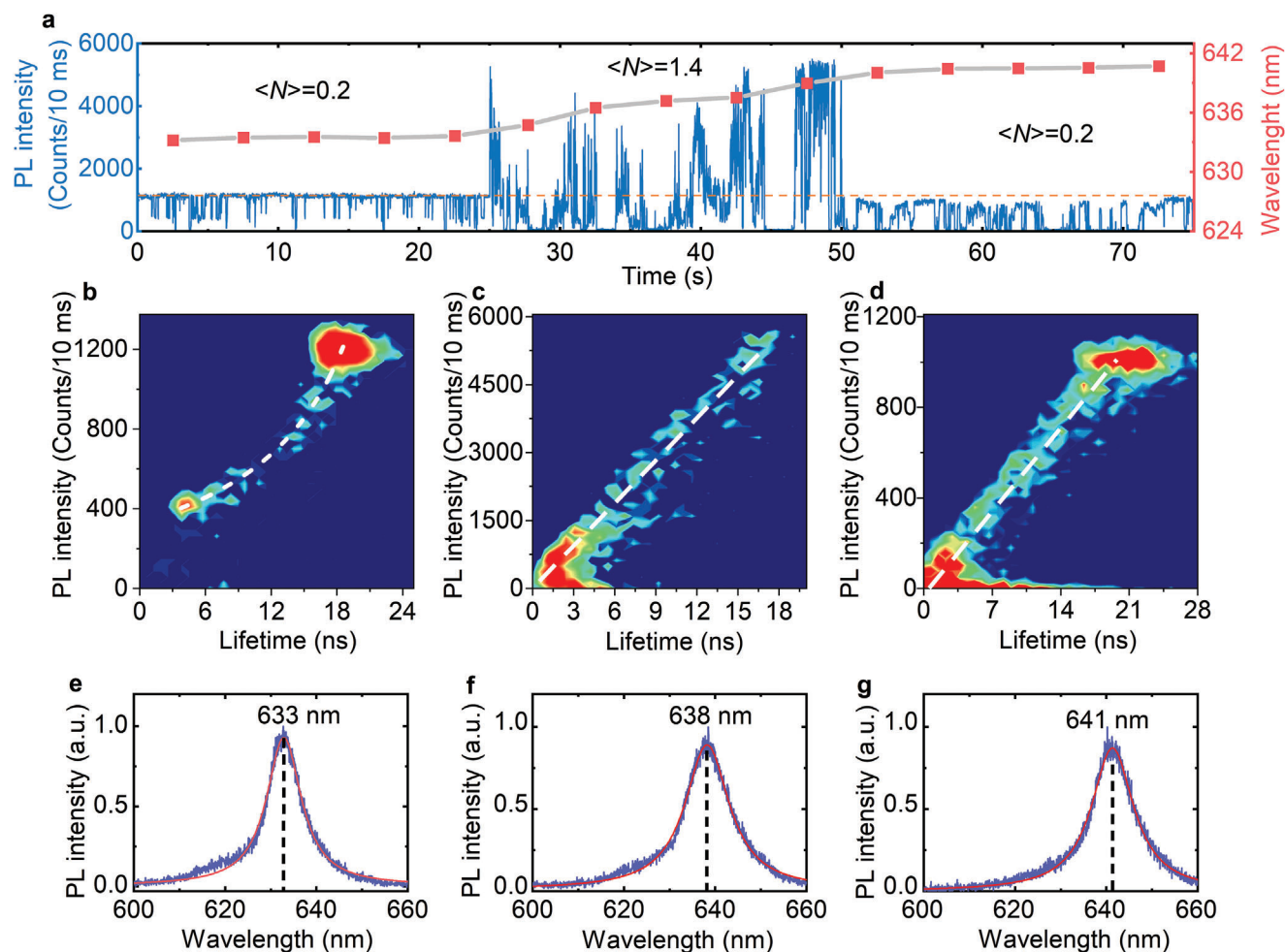
Figure 2. Conversion of blinking types in single alloyed CdSe/ZnS QDs. a) Typical PL intensity trajectory of single alloyed CdSe/ZnS QDs and corresponding PL spectral peak positions, when <N> increases from 0.2 to 1.4, and then back to 0.2. b–d) Corresponding FLID maps at <N> = 0.2, 1.4, and 0.2. The white dotted lines are the simulated lines and derived from Equations 1 and 2, respectively. e–g) Corresponding PL spectra were recorded at 10–15, 35–40, and 60–65 s, respectively. The red curves are Gaussian fits.

MRC model of BC-blinking, the different intensity levels in the BC-blinking trajectory is caused by the fluctuating non-radiative rates ($k_{nr}(t)$) and a fixed radiative rate, resulting in a linear correlation between the PL intensity and the PL lifetime. This correlation is expressed by:[13,14]

$$I \propto QY = \frac{k_r}{k_r + k_{nr}(t)} = \tau k_r = \frac{\tau}{\tau_r} \quad (2)$$

The FLID map in the right panel of Figure 1d can be simulated well by Equation 2, as shown by the white dotted line, indicating that the observed PL blinking is a pure BC-blinking. In the BC-blinking, the intermittency of the PL emission originates from the fluctuating non-radiative rate of single excitons due to the activation and deactivation of a set of non-radiative centers, as schematically shown in Figure 1f. In addition, the ratios of radiative rates between various PL regions in the PL intensity trajectory of Figure 1d are calculated to be ≈1 (Figure S6, Supporting Information), which also confirms that the observed blinking is BC-blinking.

2.2. Conversion of Blinking Types in Single Alloyed CdSe/ZnS QDs

We investigate the PL blinking behavior of alloyed CdSe/ZnS QDs with different surface ligands, particle sizes and shell thicknesses. It is found that the blinking behavior of single alloyed CdSe/ZnS QDs with a shell thickness of up to 2 nm undergoes an irreversible conversion from Auger-blinking to BC-blinking. Here, alloyed CdSe/ZnS core/shell QDs with a shell thickness of ≈2.0 nm are used as an example to present the blinking type conversion. A typical PL intensity trajectory of single alloyed CdSe/ZnS QDs and corresponding PL spectral peak positions are shown in **Figure 2a**, where <N> increases from 0.2 to 1.4, and then back to 0.2. Corresponding PL lifetime trajectory is shown in Figure S7 (Supporting Information). Corresponding $g^{(2)}$ curves under different excitation conditions indicate that the investigated QD is indeed single nanoparticle (Figure S8a–c, Supporting Information). Figure 2b–d show the corresponding FLID maps. Equation 1 can well simulate the curved FLID map for the PL intensity trajectory of 0 – 25 s (<N> = 0.2) (Figure 2b), indicating
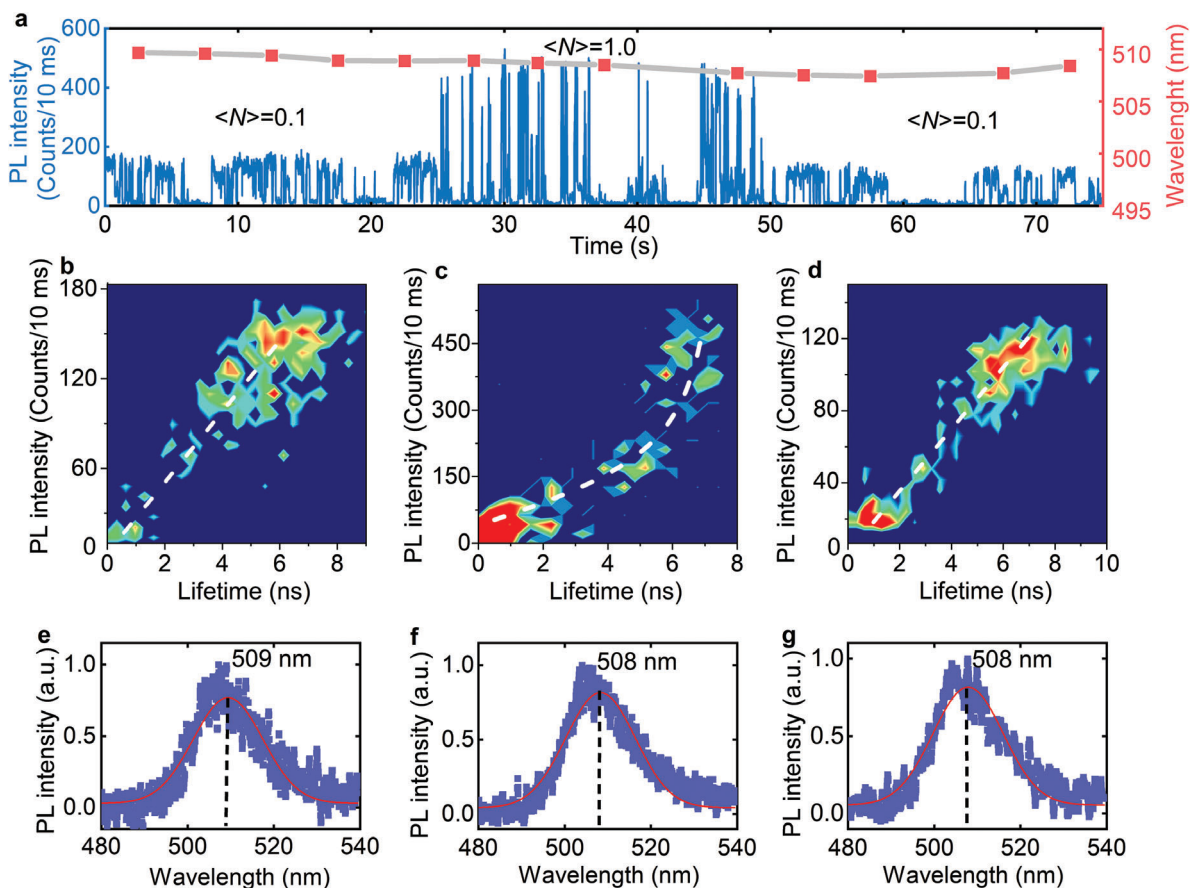
**ADVANCED
SCIENCE NEWS**

www.advancedsciencenews.com

NANO · MICRO

small

www.small-journal.com

Figure 3. Conversion of blinking types in single $CH_3NH_3PbBr_3$ perovskite QDs. a) Typical PL intensity trajectory of single $CH_3NH_3PbBr_3$ perovskite QDs and corresponding PL spectral positions, when <*N*> increases from 0.1 to 1.0, and then back to 0.1. b–d) Corresponding FLID maps at <*N*> = 0.1, 1.0, and 0.1. The white dotted lines are the simulated lines, given by Equations 2 and 3, respectively. e–g) Corresponding PL spectra were recorded at 10–15, 35–40, and 60–65 s, respectively. The red curves are Gaussian fits.

that the PL blinking is Auger-blinking. When <*N*> increases to 1.4, the FLID map changes from curved to linear (Figure 2c), indicating that the PL blinking changes from Auger-blinking to BC-blinking. It is noteworthy that upon decreasing <*N*> back to 0.2, the FLID map remains linear, as indicated by Figure 2d. This implies that the conversion of blinking types in the single alloyed CdSe/ZnS QDs is irreversible upon a change in excitation conditions. Furthermore, the PL spectra recorded at 10–15, 35–40, and 60–65 s under the three different <*N*> values, show a redshift from 633 to 641 nm, as shown in Figure 2e–g. The average redshift observed in the PL spectra of ≈100 single QDs is ≈6.5 nm as displayed in Figure S9 (Supporting Information). The conversion of blinking types and spectral redshift may be related to the release of coherency strain at the QD core/shell interface or a change in interface potential under the increased laser fluence. This will be further discussed in the subsequent section.

2.3. Conversion of Blinking Types in Single $CH_3NH_3PbBr_3$ Perovskite QDs

We investigate the PL blinking behavior of perovskite QDs with different particle sizes and compositions. It is found that single

perovskite QDs with particle sizes smaller than their Bohr diameters exhibit reversible conversion between BC-blinking and more pronounced Auger-blinking. Here, single $CH_3NH_3PbBr_3$ perovskite QDs with particle size of ≈3.2 nm are used as an example to present the conversion of blinking types. The particle size of ≈3.2 nm is smaller than its exciton Bohr diameter of 4 nm.[26] A typical PL intensity trajectory of single $CH_3NH_3PbBr_3$ perovskite QDs and corresponding PL spectral positions are shown in **Figure 3**a, where we change <*N*> from 0.1 to 1.0, and then back to 0.1. The corresponding PL lifetime trajectory is shown in Figure S10 (Supporting Information). The corresponding $g^{(2)}$ curves under different excitation conditions indicate that the studied QD is a single QD (Figure S8d–f, Supporting Information). The FLID map of $CH_3NH_3PbBr_3$ perovskite QDs can change from linear to nonlinear when <*N*> increases from 0.1 to 1.0 (Figure 3b,c), and then resumes to linear when <*N*> drops back to 0.1 (Figure 3d). This indicates that the blinking type of single $CH_3NH_3PbBr_3$ perovskite QDs can undergo a reversible conversion by changing <*N*>. The corresponding PL spectra recorded at 10–15, 35–40, and 60–65 s illustrate that the PL spectral peak positions remain almost the same during the blinking type conversions, as shown in Figure 3e–g. Nonetheless, we notice that the curved FLID map in Figure 3c cannot be

**ADVANCED
SCIENCE NEWS**

www.advancedsciencenews.com

NANO · MICRO

small

www.small-journal.com

simulated well using Equation 1, and the curvature of the simulated curve is greater than that of the FLID map, as depicted by the yellow dotted line in Figure S12 (Supporting Information) (see Section S1, Supporting Information for details). This excludes the scenario where Auger-blinking is the only mechanism of PL blinking. Thus, we assume that Auger-blinking and BC-blinking coexist in the QD. By considering the coexistence of the two blinking mechanisms, Equation 3 can be constructed.

$$I = A_{Auger} \frac{I_1 I_2 (\tau_2 - \tau_1)}{I_2 (\tau_2 - \tau) + I_1 (-\tau_1 + \tau)} + A_{BC} \frac{\tau}{\tau_r} \quad (3)$$

where the first term represents the contribution of the Auger-blinking mechanism, the second term represents the contribution of BC-blinking mechanism, and A_{Auger} and A_{BC} are the corresponding amplitudes of each component. The FLID map in Figure 3c can be well simulated using Equation 3. This sound simulation indicates that Auger-blinking and BC-blinking mechanisms are both present in the single perovskite QD at the higher excitation conditions. According to the simulation, we obtain A_{Auger}: $A_{BC} \approx 3$: 1, suggesting that Auger-blinking dominates the PL blinking at higher excitation conditions. Therefore, the blinking type of single $CH_3NH_3PbBr_3$ perovskite QDs can be converted reversibly between the BC-blinking and the more prominent Auger-blinking by altering the excitation conditions.

2.4. Analysis of Blinking Type Conversion for Alloyed CdSe/ZnS QDs

To investigate the conversion of blinking types in single alloyed CdSe/ZnS QDs, we must first explore the origin of Auger-blinking at low excitation conditions. Auger-blinking typically arises from two distinct charging channels: the single exciton ionization and the Auger ionization of multiexciton (mainly biexcitons).[14,15] This can be determined by examining the correlation between charging rate and excitation condition <N>. Single exciton ionization results in a linear correlation between charging rate and <N>,[14] while Auger ionization of multiexciton results in a quadratic relationship between the charging rate and <N>.[15] The charging rate of single QDs can be calculated according to $r_c = N_{(N \to c)}/t_N$,[15] where $N_{(N \to c)}$ represents the total number of "neutral exciton state to charged state" events, and t_N is the total duration of neutral exciton state in the PL blinking trajectory. By analyzing the charging rates of blinking trajectories of single alloyed CdSe/ZnS QDs under different excitation conditions (<N> = 0.03 – 0.3), we observed a linear correlation between the charging rate and <N>, as shown in **Figure 4** (detailed analysis presented in Figure S13, Supporting Information). The linear correlation indicates that the charging of QDs is relevant to single exciton ionization. Single exciton ionization occurs when a photoexcited carrier escapes from a single exciton and is captured by a long-lived trap of the QDs, and the remaining counter-charge subsequently quenches the PL emission by non-radiative Auger recombination,[14,39] as illustrated in **Figure 5a**. The long-lived traps in the alloyed CdSe/ZnS QDs are believed to arise from the surface defects.[14] Due to the relatively thick ZnS shell (2 nm) present in the alloyed CdSe/ZnS QDs, there is a weak overlap of wave functions between the surface defects and
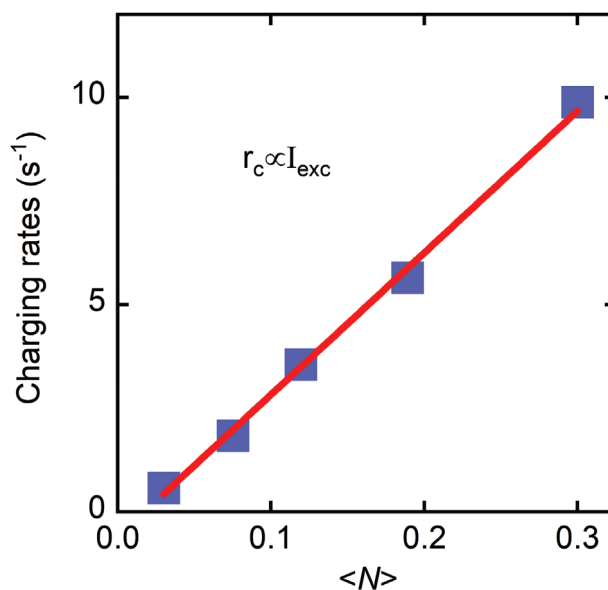

Figure 4. Dependence of charging rate on excitation condition <N> for single alloyed CdSe/ZnS QDs.

excitons (blue shadow in left panel of Figure 5b). Because of the weak overlap of wave functions, the surface defects trap and detrap carriers at a slow rate, resulting in the surface defects behaving as long-lived traps that are responsible for the Auger-blinking. Here, we classify traps as either long-lived or short-lived based on the degree of wave function overlap with the excitons. When the wave function overlap is weaker, the trapping and de-trapping rates are slower, resulting in Auger-blinking, which is defined as a long-lived trap. On the other hand, greater wave function overlap leads to faster trapping and de-trapping rates, resulting in BC blinking, which is defined as a short-lived trap.

As previously shown, under higher excitation conditions, the blinking of single alloyed CdSe/ZnS QDs can be irreversibly converted from Auger-blinking to BC-blinking, which is accompanied by a redshift in the PL spectrum. In this section, we analyze the potential causes of the blinking type conversion. As mentioned earlier, fluctuations in the nonradiative rate of single excitons are caused by the activation and deactivation of a set of non-radiative recombination centers (short-lived traps), leading to BC-blinking of QDs. Thus, the conversion from Auger-blinking to BC-blinking under higher excitation conditions suggests the introduction of short-lived traps in the alloyed CdSe/ZnS core/shell QDs. It is speculated that the short-lived traps of the alloyed CdSe/ZnS QDs may originate from newly created interfacial defects, for the following reasons: Despite the alloying of the CdSe/ZnS QDs, a lattice mismatch may still exist at the core/shell interface, leading to coherency strain.[42] Dislocations may form at the core/shell interface due to the release of coherency strain caused by high laser fluence, resulting in the formation of interfacial defects.[43] Due to the absence of a shell barrier between excitons and interfacial defects, there is a significant overlap of wave functions between them, as illustrated by the pink shadow in the right panel of Figure 5b. The significant overlap of wave functions enables interfacial defects to trap and de-trap carriers rapidly, thereby behaving as short-lived traps.
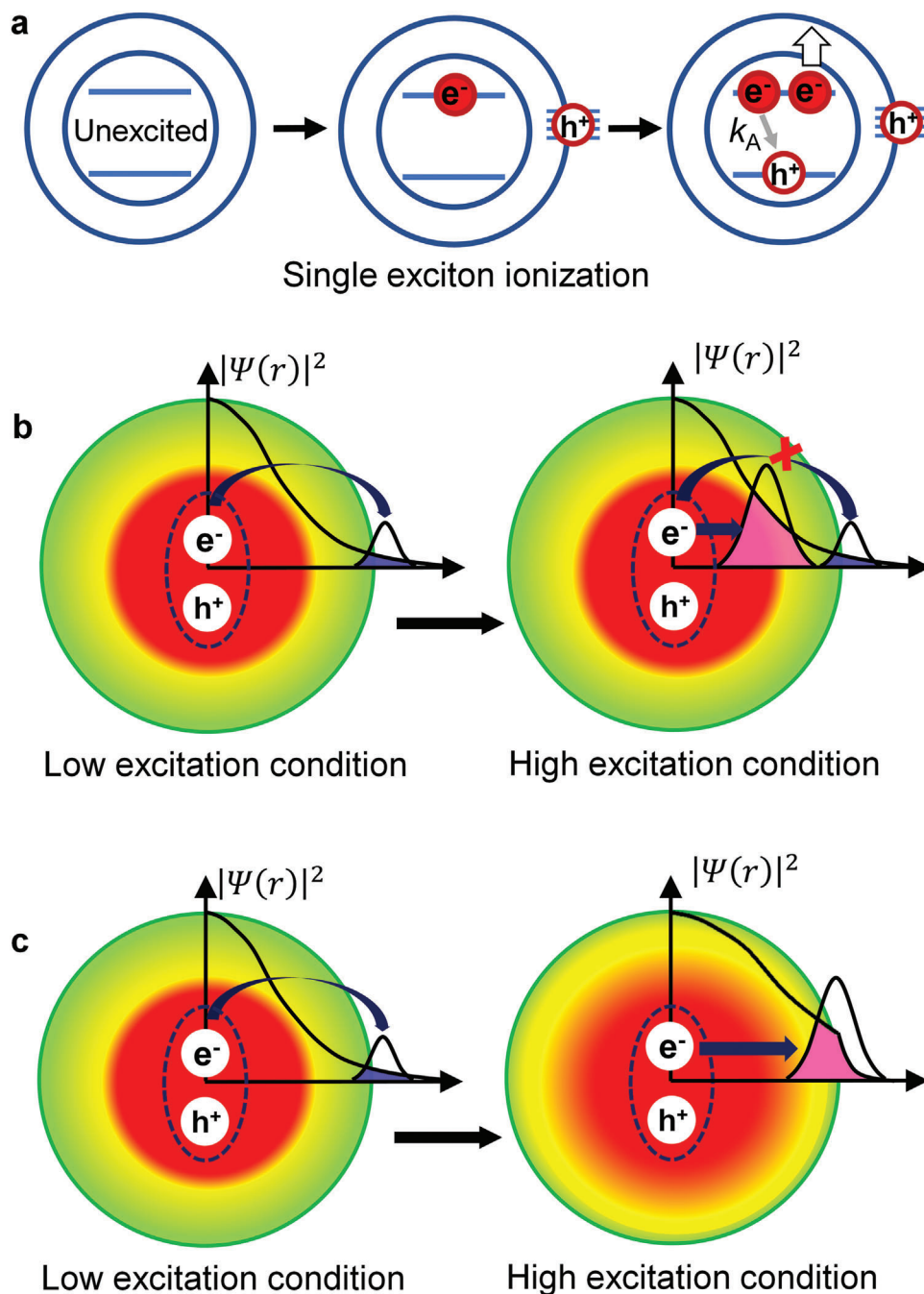
ADVANCED
SCIENCE NEWS
www.advancedsciencenews.com

NANO · MICRO
small
www.small-journal.com

Figure 5. Schematic diagrams of the charging processes and the blinking type conversions of alloyed CdSe/ZnS QDs. a) Schematic of single exciton ionization in single alloyed CdSe/ZnS QDs under the low excitation conditions. b) Conversion of blinking types in single alloyed CdSe/ZnS QDs from Auger-blinking to BC-blinking due to newly created interfacial defects under high excitation conditions. Blue shading represents the wave function overlap between excitons and long-lived traps, and pink shading represents the wave function overlap between excitons and shot-lived traps. c) Conversion of blinking types in single alloyed CdSe/ZnS QDs from Auger-blinking to BC-blinking due to the further smoothing of core/shell interface potential resulting in a larger overlap of wave functions between excitons and surface defects.

As previously stated, both Auger-blinking and BC-blinking in alloyed CdSe/ZnS QDs result from the trapping of carriers in single excitons. The significant overlap of wave functions between single excitons and interfacial defects results in carriers in single excitons being preferentially captured by the interfacial defects. Therefore, the interfacial defects take priority over the surface

defects as new effective trapping sites to be responsible for the blinking of the alloyed CdSe/ZnS. This leads to the conversion of blinking type from Auger-blinking to BC-blinking.

Furthermore, the generation of interfacial defects is also supported by the decrease in single-QD PL intensity after high-power laser irradiation, as illustrated in Figure 2a. The PL intensity at

50 – 75 s after high-power laser irradiation is 15% lower than the initial intensity at 0 – 25 s, as indicated by the yellow dotted line in the figure. According to the statistical analysis of ≈100 single QDs, their average PL intensity reduction is ≈10%, as depicted in Figure S14 (Supporting Information). This is consistent with previous reports that the PLQY of alloyed CdZnSeS/ZnS core/shell QDs can be reduced after high-power laser irradiation and has also been attributed to the generation of interfacial defects.[43,44] Additionally, the appearance of interfacial defects can cause an increase in PL blinking of the alloyed CdSe/ZnS QDs. The PL blinking that occurs between 50 – 75 s after high-power laser irradiation are more frequent than the initial blinking that occurs between 0 – 25 s (Figure 2a). The blinking rate, defined as the number of blinking events per second,[45] increased from 2.8 to 3.4 s^{-1}. This could potentially be attributed to the increased occurrence of carrier traps resulting from greater overlap of wave functions between excitons and interfacial traps.[46] In addition, the release of coherency strain can alter the crystal potential and change the band structure,[42,47,48] causing the PL spectrum redshift.

The high-power laser irradiation may also induce the further smoothing of core/shell interface potential, which can also explain the conversion of PL blinking types in the CdSe/ZnS QDs. Exposure of CdSe/ZnS core/shell QDs to high laser fluences induces interdiffusion of Se and S elements at the core/shell interface,[30,49] resulting in interface alloying and ultimately smoothing of the core/shell interface potential.[30,48] Therefore, it is possible that a similar phenomenon could occur in our CdSe/ZnS QD sample under high laser fluence, which could result in an additional improvement in interface potential smoothness. The improvement in interface potential smoothness softens the exciton confinement potential, making it easier for the exciton wave function to delocalize to the QD surface. This results in a larger overlap of wave functions between excitons and surface defects (Figure 5c). As a result, the surface defects behavior changes from long-lived traps to short-lived traps, causing the blinking type conversion from Auger-blinking to BC-blinking. Moreover, the exciton confinement potential softening can also result in a redshift of the PL spectrum.[43,50]

2.5. Analysis of Blinking Type Conversion for CH$_3$NH$_3$PbBr$_3$ Perovskite QDs

As previously shown, single CH$_3$NH$_3$PbBr$_3$ perovskite QDs exhibit BC-blinking at low excitation conditions, and their PL blinking type can convert from BC-blinking to more prominent Auger-blinking with the increasing laser fluence. We first investigate the origin of BC-blinking of single CH$_3$NH$_3$PbBr$_3$ perovskite QDs under low excitation conditions. The BC-blinking in CH$_3$NH$_3$PbBr$_3$ perovskite QDs originates from short-lived traps that arise from surface defects.[25,51] The compact size and shell-free structure of the CH$_3$NH$_3$PbBr$_3$ perovskite QDs lead to a significant wave function overlap between surface defects and excitons (the left panel of **Figure 6**b). This significant overlap enables surface defects to function as short-lived traps, allowing for the quick trapping and de-trapping carriers in excitons, resulting in BC-blinking. Surface defects in perovskite QDs are believed to originate from surface uncoordinated lead (dangling

bonds),[25,34,51,52] which has been confirmed by the observation of suppressed blinking after the elimination of dangling bonds with thiocyanate or alkylthiols.[25,34,51,53–57]

Under higher excitation conditions, single CH$_3$NH$_3$PbBr$_3$ perovskite QDs exhibit more pronounced Auger-blinking. The origin of the Auger-blinking in single CH$_3$NH$_3$PbBr$_3$ perovskite QDs can be determined by measuring the charging rate dependence on $<N>$. Regrettably, under high excitation conditions, the PL intensity trajectories of single CH$_3$NH$_3$PbBr$_3$ perovskite QDs are highly disordered, thus making it challenging to determine the correlation between the charging rate and $<N>$. However, considering the two facts that more multiexcitons are generated under high excitation conditions, and that the Auger recombination process is more efficient within the small-sized perovskite QDs,[33,37] the Auger-blinking of CH$_3$NH$_3$PbBr$_3$ perovskite QDs should originate from the Auger ionization of multiexcitons. Long-lived traps are necessary for Auger-blinking as stated earlier. However, the small size of the CH$_3$NH$_3$PbBr$_3$ perovskite QD sample makes it improbable to have long-lived traps present.[52,58,59] Therefore, the charging of the CH$_3$NH$_3$PbBr$_3$ perovskite QDs is most likely caused by the Auger ionization-assisted ejection of one carrier from the QD into the surface ligands[51] or the surrounding matrix,[5,60] as depicted in Figure 6a. The acceptor-like sites on surface ligands and surrounding matrix have a slow de-trapping rate due to the weak wave function overlap between excitons and acceptor-like sites (blue shadow in the right panel of Figure 6b), so acceptor-like sites can behave as long-lived traps and cause Auger-blinking. In contrast to the alloyed CdSe/ZnS QDs, the BC-blinking and Auger-blinking in CH$_3$NH$_3$PbBr$_3$ perovskite QDs originate from two distinct pathways: The BC-blinking arises from the trapping of carriers in single exciton by short-lived surface defects, while Auger-blinking arises from the trapping of carriers in multiexciton by long-lived acceptor-like sites, as depicted in Figure 6b. Under high excitation conditions, the short-lived surface defects and the long-lived acceptor-like sites can concurrently participate in the PL blinking process as effective trapping sites for carriers. This results in the coexistence of both BC-blinking and Auger-blinking in the CH$_3$NH$_3$PbBr$_3$ perovskite QDs. Furthermore, the reason for perovskite QDs exhibiting more pronounced Auger-blinking is the increased Auger ionization of multiexcitons under high excitation conditions.

2.6. Conversion of Blinking Types in Other QDs with Different Surface Ligands, Particle Sizes, Shell Thicknesses and Compositions

Additionally, we conducted experiments to investigate the conversion of blinking types in alloyed CdSe/ZnS QDs with varied surface ligands, particle sizes and shell thicknesses, as well as those of other perovskite QDs with different compositions and particle sizes (details can be found in Sections S2 and S3, Supporting Information). We can observe a similar blinking type conversion from Auger-blinking to BC-blinking in alloyed CdSe/ZnS QDs with different surface ligands (oleic acid, oleylamine and 1-octanethiol), implying that the surface ligands have little effect on the blinking type conversion behavior (Figure S16, Supporting Information). Similarly, single alloyed CdSe/ZnS QDs with
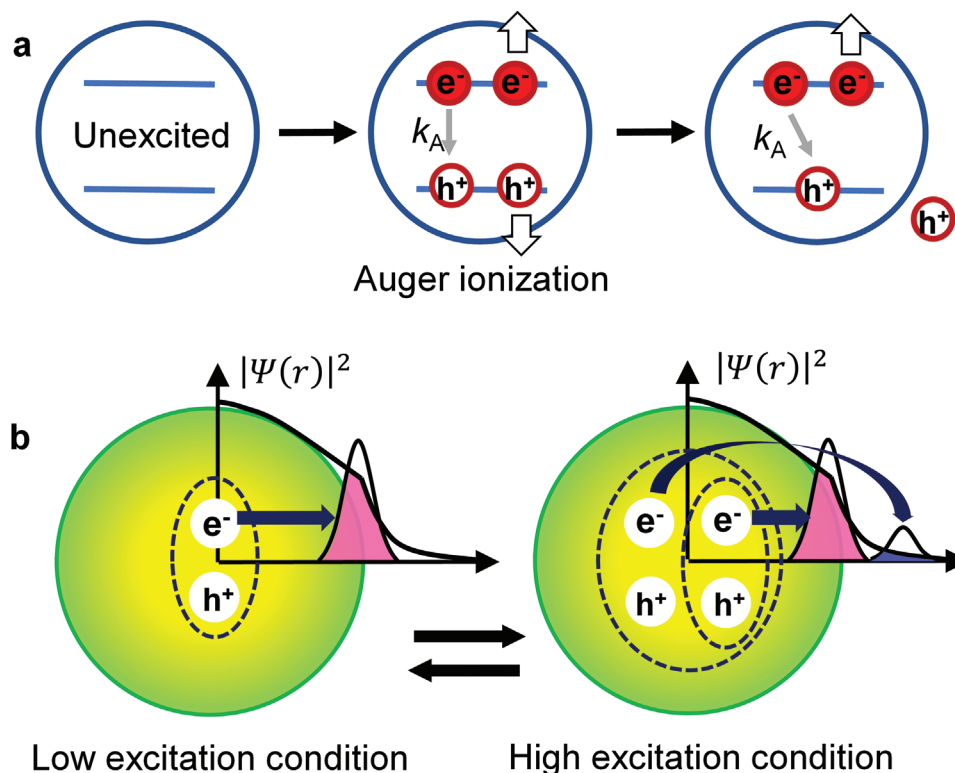
ADVANCED
SCIENCE NEWS

www.advancedsciencenews.com

NANO · MICRO
small
www.small-journal.com

Figure 6. Schematic diagrams of the charging processes and the blinking type conversions of $CH_3NH_3PbBr_3$ perovskite QDs. a) Schematic of Auger ionization of multiexciton in single $CH_3NH_3PbBr_3$ perovskite QDs under high excitation conditions. b) Conversion of blinking types in single $CH_3NH_3PbBr_3$ perovskite QDs from BC-blinking to more pronounced Auger-blinking due to the Auger ionization of multiexcitons leading to carrier trapping by long-lived acceptor-like sites on the surface ligands and surrounding matrix under high excitation conditions. Pink shading represents the wave function overlap between excitons and shot-lived traps, and blue shading represents the wave function overlap between excitons and long-lived traps.

thicker shell of ≈3 nm also exhibit the PL blinking type conversion from Auger-blinking to BC-blinking with the increasing laser fluence (Figure S18, Supporting Information), which is the same as the alloyed CdSe/ZnS QDs with ≈2 nm shell thickness studied above. It is important to note that the PL blinking behavior of the alloyed CdSe/ZnS QDs changes significantly as the shell thickness decreases. Under low excitation conditions, the thinner shell alloyed CdSe/ZnS QDs (1.2 and 0.7 nm) are more inclined to show BC-blinking rather than Auger-blinking (Figure S19, Supporting Information). This phenomenon can be attributed to the increased wave function overlap between the surface defects and excitons due to the thinner shell. The increased overlap allows the surface defects to act as short-lived traps, resulting in BC-blinking. Furthermore, the BC-blinking of CdSe/ZnS QDs does not convert to Auger-blinking as the laser fluence increases (Figure S19, Supporting Information). This is in contrast to the $CH_3NH_3PbBr_3$ perovskite QDs. The reason for not observing a blinking type conversion from BC-blinking to Auger-blinking may be attributed to the effective suppression of Auger ionization of multiexcitons by the alloyed structure in CdSe/ZnS QDs.[8,49,61] We have also investigated the blinking behavior of small-sized alloyed CdSe/ZnS QDs (particle size of QDs is ≈3.9 nm, and ZnS shell thickness is ≈1 nm) (Figure S20, Supporting Information). Small-sized CdSe/ZnS QDs typically exhibit a BC-blinking behavior under weak excitation conditions. However, it is difficult to observe the blinking conversion

of small-sized QDs at higher excitation conditions due to photobleaching of the QDs. The small-sized CdSe/ZnS QDs should be like the CdSe/ZnS QDs mentioned above that show BC-blinking, which does not convert to Auger-blinking because the alloyed structure in small-sized CdSe/ZnS QDs effectively suppresses the Auger ionization of multiexcitons. All experimental results on alloyed CdSe/ZnS QDs with varying surface ligands and shell thicknesses have been summarized in Table S1 (Supporting Information) for easy reference.

For the investigation of blinking type conversions of other perovskite QDs, perovskite QD samples of $CsPbBr_3$ and $CsPbI_3$ with varying particle sizes were synthesized. In contrast to the $CH_3NH_3PbBr_3$ perovskite QDs, the particle sizes of these all-inorganic $CsPbBr_3$ and $CsPbI_3$ perovskite QDs are easier to be controlled.[62] Our investigations show that the PL blinking behavior of $CsPbBr_3$ and $CsPbI_3$ perovskite QDs with particle sizes smaller than their Bohr diameters (7 and 12 nm, respectively) are similar to that of $CH_3NH_3PbBr_3$ perovskite QDs studied above, where most $CsPbBr_3$ and $CsPbI_3$ perovskite QDs exhibit BC-blinking under low excitation conditions, which can also convert to more pronounced Auger-blinking as the laser pump fluence increases (Figures S22 and S24, Supporting Information). It is worth noting that perovskite QDs with sizes larger than their Bohr diameters can show Auger-blinking under low excitation conditions (Figures S22 and S24, Supporting Information). The larger particle size can reduce the wave function overlap between

ADVANCED
SCIENCE NEWS

www.advancedsciencenews.com

NANO · MICRO
small
www.small-journal.com

excitons and surface defects. This leads to the surface defects behaving as long-lived traps. Thus, the perovskite QDs with larger particle sizes can exhibit Auger-blinking under low excitation conditions. We also investigated the blinking type conversion behavior in large-size perovskite QDs under high excitation conditions. According to the experimental observations, the blinking type of large-size perovskite QDs remains as Auger-blinking and does not convert to BC-blinking, even when the excitation condition <N> increases to 2.5 (see Figure S25, Supporting Information). This is due to the absence of a core/shell structure in perovskite QDs, which does not allow for the generation of new effective trapping sites or smoothing of interface potential. These findings also confirm that the core/shell interface (including interfacial defects and interface potential) is crucial for the PL blinking type conversion in alloyed CdSe/ZnS QDs. Table S3 (Supporting Information) summarizes all experimental findings on perovskite QDs with varying particle sizes.

3. Conclusion

We have investigated the blinking behavior of alloyed CdSe/ZnS QDs with different surface ligands, particle sizes and shell thicknesses, as well as perovskite QDs with various compositions and particle sizes. Using FLID map simulation, pure BC blinking or Auger blinking or a mixture of both blinking behaviors have been identified in these QDs. It is found that the blinking types of some QDs can be converted by tuning the laser pump fluence. Single alloyed CdSe/ZnS QDs with a shell thickness of up to 2 nm exhibit an irreversible conversion of their blinking type from Auger blinking to BC blinking as the laser fluence increases. The alloyed CdSe/ZnS QDs with a thinner shell are more inclined to show BC-blinking, without converting to Auger-blinking with the change of laser fluence. Single perovskite QDs, having particle sizes smaller than their Bohr diameters, exhibit a reversible blinking type conversion between BC-blinking and a more pronounced Auger-blinking. Single perovskite QDs with particle sizes larger than their Bohr diameters exhibit Auger-blinking under low excitation conditions, but their blinking type remains Auger-blinking and does not convert to BC-blinking even under very high excitation conditions. Consequently, the thickness of QD shells and the size of particles have a significant effect on the conversion of blinking types. This is because they can alter the overlap of the wave functions between the excitons and the effective trapping sites, making the effective trapping sites behave as either long-lived or short-lived traps. Upon analysis of the origins of blinking under different excitation conditions, it is found that changes in the effective trapping sites under different excitation conditions are responsible for the conversion of PL blinking types. For instance, a change in the effective trapping sites from long-lived traps to short-lived traps can result in the conversion of blinking type from Auger-blinking to BC blinking. The conversion of blinking types under different excitation conditions can well explain that the QDs with the same chemical compositions and from the same synthesis batch show different blinking types. The study elucidates the discrepancies in the blinking behavior of various QD samples observed in previous reports, and provides insights into the mechanisms for different types of blinking under different excitation conditions,

opening up the possibility of fabricating advanced QD materials with a wide range of applications.

4. Experimental Section

Synthesis of Alloyed CdSe/ZnS QDs: The alloyed CdSe/ZnS QDs with gradient chemical composition were synthesized by the traditional "hot injection" method.[63] In a typical synthesis, 0.4 mmol CdO, 10 mmol $Zn(OAc)_2$, and 15 mL oleic acid (OA) were loaded into a 100 mL three-necked flask, after degassing at 120 °C for 40 min, a mixture of $Zn(OA)_2$ and $Cd(OA)_2$ precursors was obtained. Then 30 mL 1-octadecene (ODE) was added to the flask and the solution was heated to 320 °C under an argon atmosphere. Then the Se precursor (0.8 mmol Se dissolved in 0.4 mL trioctylphosphine (TOP)) was rapidly injected into the flask and the solution was kept for 30 min to obtain the alloyed cores. The temperature was then set at 310 °C and another Se precursor solution (0.5 mmol Se dissolved in 0.25 mL TOP) was added to the flask. The solution was kept for 10 min to allow the intermediate layer to grow. Then the Cd precursor solution (1.4 mmol $Cd(OA)_2$ in 7 mL ODE) and the S precursor solution (2.8 mmol S in 1.4 mL TOP) were simultaneously added dropwise to the flask at 280 °C at a rate of 10.5 and 2.1 mL h^{-1}, respectively, to achieve growth of the CdZnS shell. Finally, the S precursor solution (1.0 mmol S in 0.5 mL TOP) was added to the flask and the solution was kept for 20 min to achieve the growth of the ZnS shell. When the desired alloyed CdSe/ZnS QDs were obtained, the solution was cooled to room temperature by an ice bath. The resulting alloyed CdSe/ZnS QDs with OA ligands were washed 3 times with ethanol and dispersed in heptane. For simplicity, the alloy core and intermediate layer were referred to collectively as the core, and the CdZnS and ZnS layers were referred to collectively as the shell. In addition, in order to obtain a higher PLQY, a ligand exchange process was applied to replace the surface ligands of the QDs from the original OA to 1-octanethiol. The detailed procedure was as follows: The purified CdSe/ZnS QDs with OA ligands were first dissolved in chlorobenzene. A certain amount of 1-octanethiol was then added to the solution. After continuous stirring for 14 h at 50 °C under an argon atmosphere, the obtained CdSe/ZnS QDs with 1-octanethiol ligands were washed with ethanol and dispersed in heptane. Similarly, alloyed CdSe/ZnS QDs with oleylamine ligands could also be obtained by the ligand exchange reaction.

Synthesis of $CH_3NH_3PbBr_3$ Perovskite QDs: The preparation of $CH_3NH_3PbBr_3$ perovskite QDs was based on the emulsion synthesis method.[32] First, 0.2 mmol $PbBr_2$ and 0.16 mmol CH_3NH_3Br were dissolved in 0.5 mL N,N-dimethylformamide (DMF) and 0.3 mL DMF, respectively, to obtain the precursor solution. The two precursor solutions were then added dropwise to the mixture of 10 mL toluene, 0.5 mL oleic acid, and 20 μL n-octylamine to form an emulsion. A demulsification process was then initiated by adding 8 mL of acetonitrile (demulsifier) to the emulsion. Finally, by centrifugation at 6000 rpm for 5 min, the solvents and excess reactants were discarded as supernatant, and the precipitates were dispersed in toluene to obtain the $CH_3NH_3PbBr_3$ perovskite QDs solution.

Preparation of Single QDs Samples: For single QDs measurements, the QD solution was typically diluted to ≈10^{-9} mol L^{-1}, and the solution was then spin-coated onto clean glass coverslips at a rotation speed of 3000 rpm for 1 min. In addition, to protect the single perovskite QDs, ≈1 wt.% polystyrene was mixed in the diluted solution prior to spin coating.

Experimental Setup: A home-built confocal scanning fluorescence imaging microscope was used for single QD measurements. In our study, the QDs were excited using a supercontinuum laser (NKT Photonics, EXW-12) with an output pulse width of 50–100 ps. Single CdSe/ZnS QDs were excited by the laser at a wavelength of 532 nm and a repetition rate of 5 MHz. Single $CH_3NH_3PbBr_3$ perovskite QDs were excited by the laser at a wavelength of 439 nm and a repetition rate of 10 MHz. An oil immersion objective (OLYMPUS, 100×, 1.3NA) was mounted in an inverted microscope (OLYMPUS, IX71) to focus the laser beam and simultaneously

**ADVANCED
SCIENCE NEWS**

www.advancedsciencenews.com

NANO · MICRO
small

www.small-journal.com

collect the PL of single QDs. Finally, two single-photon detectors (Excelitas, SPCM-AQRH-16-FC) were used to detect the PL photons according to the HBT scheme. The arrival time of each detected photon and the corresponding synchronization of the pulsed laser were recorded by a time-tagged time-resolved time-correlated single-photon counting (TTTR-TCSPC) data acquisition card (SIMINICS, FT1040). In addition, the PL spectra of single QDs were recorded by a spectrometer (ANDOR, shamrock500i) with an EMCCD camera (ANDOR, Newton 940).

Supporting Information

Supporting Information is available from the Wiley Online Library or from the author.

Conflict of Interest

The authors declare no conflict of interest.

Author Contributions

All authors commented on the manuscript. The manuscript was prepared with the contributions of all authors. All authors agree to the final version of the manuscript.

Data Availability Statement

The data that support the findings of this study are available from the corresponding author upon reasonable request.

Keywords

blinking mechanisms, blinking type conversion, CdSe/ZnS quantum dots, perovskite quantum dots, photoluminescence blinking

[1] J. M. Pietryga, Y.-S. Park, J. Lim, A. F. Fidler, W. K. Bae, S. Brovelli, V. I. Klimov, *Chem. Rev.* **2016**, *116*, 10513.

[2] J. Y. Kim, J.-W. Lee, H. S. Jung, H. Shin, N.-G. Park, *Chem. Rev.* **2020**, *120*, 7867.

[3] Y. Yuan, N. Jin, P. Saghy, L. Dube, H. Zhu, O. Chen, *J. Phys. Chem. Lett.* **2021**, *12*, 7180.

[4] C. Wu, K. Wang, Y. Zhang, X. Zhou, T. Guo, *J. Phys. Chem. Lett.* **2021**, *12*, 3522.

[5] M. Nirmal, B. O. Dabbousi, M. G. Bawendi, J. J. Macklin, J. K. Trautman, T. D. Harris, L. E. Brus, *Nature* **1996**, *383*, 802.

[6] H. Qin, Y. Niu, R. Meng, X. Lin, R. Lai, W. Fang, X. Peng, *J. Am. Chem. Soc.* **2014**, *136*, 179.

[7] O. Chen, J. Zhao, V. P. Chauhan, J. Cui, C. Wong, D. K. Harris, H. Wei, H.-S. Han, D. Fukumura, R. K. Jain, M. G. Bawendi, *Nat. Mater.* **2013**, *12*, 445.

[8] M. Nasilowski, P. Spinicelli, G. Patriarche, B. Dubertret, *Nano Lett.* **2015**, *15*, 3953.

[9] A. L. Efros, D. J. Nesbitt, *Nat. Nanotechnol.* **2016**, *11*, 661.

[10] Z. Popovic, W. Liu, V. P. Chauhan, J. Lee, C. Wong, A. B. Greytak, N. Insin, D. G. Nocera, D. Fukumura, R. K. Jain, M. G. Bawendi, *Angew. Chem., Int. Ed.* **2010**, *49*, 8649.

[11] L. A. Lane, A. M. Smith, T. Lian, S. Nie, *J. Phys. Chem. B* **2014**, *118*, 14140.

[12] A. L. Efros, M. Rosen, *Phys. Rev. Lett.* **1997**, *78*, 1110.

[13] P. A. Frantsuzov, S. Volkán-Kacsó, B. Jankó, *Phys. Rev. Lett.* **2009**, *103*, 207402.

[14] G. Yuan, D. E. Gómez, N. Kirkwood, K. Boldt, P. Mulvaney, *ACS Nano* **2018**, *12*, 3397.

[15] R. Meng, H. Qin, Y. Niu, W. Fang, S. Yang, X. Lin, H. Cao, J. Ma, W. Lin, L. Tong, X. Peng, *J. Phys. Chem. Lett.* **2016**, *7*, 5176.

[16] F. Hu, B. Lv, C. Yin, C. Zhang, X. Wang, B. Lounis, M. Xiao, *Phys. Rev. Lett.* **2016**, *116*, 106404.

[17] X. Hou, J. Kang, H. Qin, X. Chen, J. Ma, J. Zhou, L. Chen, L. Wang, L.-W. Wang, X. Peng, *Nat. Commun.* **2019**, *10*, 1750.

[18] M. Jones, S. S. Lo, G. D. Scholes, *Proc. Natl. Acad. Sci. USA* **2009**, *106*, 3011.

[19] B. R. Fisher, H.-J. Eisler, N. E. Stott, M. G. Bawendi, *J. Phys. Chem. B* **2004**, *108*, 143.

[20] P. A. Frantsuzov, R. A. Marcus, *Phys. Rev. B* **2005**, *72*, 155321.

[21] M. Kuno, D. P. Fromm, S. T. Johnson, A. Gallagher, D. J. Nesbitt, *Phys. Rev. B* **2003**, *67*, 125304.

[22] C. Galland, Y. Ghosh, A. Steinbrück, M. Sykora, J. A. Hollingsworth, V. I. Klimov, H. Htoon, *Nature* **2011**, *479*, 203.

[23] C. T. Trinh, D. N. Minh, K. J. Ahn, Y. Kang, K.-G. Lee, *Sci. Rep.* **2020**, *10*, 2172.

[24] Y.-S. Park, S. Guo, N. S. Makarov, V. I. Klimov, *ACS Nano* **2015**, *9*, 10386.

[25] N. Yarita, H. Tahara, M. Saruyama, T. Kawawaki, R. Sato, T. Teranishi, Y. Kanemitsu, *J. Phys. Chem. Lett.* **2017**, *8*, 6041.

[26] T. Kim, S. I. Jung, S. Ham, H. Chung, D. Kim, *Small* **2019**, *15*, 1900355.

[27] H. Qin, R. Meng, N. Wang, X. Peng, *Adv. Mater.* **2017**, *29*, 1606923.

[28] X. Bai, H. Li, Y. Peng, G. Zhang, C. Yang, W. Guo, X. Han, J. Li, R. Chen, C. Qin, J. Hu, G. Yang, H. Zhong, L. Xiao, S. Jia, *J. Phys. Chem. C* **2022**, *126*, 2699.

[29] B. Li, G.-F. Zhang, R.-Y. Chen, C.-B. Qin, J.-Y. Hu, L.-T. Xiao, S.-T. Jia, *Acta Phys. Sin.* **2022**, *71*, 067802.

[30] W. Guo, J. Tang, G. Zhang, B. Li, C. Yang, R. Chen, C. Qin, J. Hu, H. Zhong, L. Xiao, S. Jia, *J. Phys. Chem. Lett.* **2021**, *12*, 405.

[31] J. Li, D. Wang, G. Zhang, C. Yang, W. Guo, X. Han, X. Bai, R. Chen, C. Qin, J. Hu, L. Xiao, S. Jia, *Nano Res.* **2022**, *15*, 7655.

[32] X. Han, G. Zhang, B. Li, C. Yang, W. Guo, X. Bai, P. Huang, R. Chen, C. Qin, J. Hu, Y. Ma, H. Zhong, L. Xiao, S. Jia, *Small* **2020**, *16*, 2005435.

[33] B. Li, H. Huang, G. Zhang, C. Yang, W. Guo, R. Chen, C. Qin, Y. Gao, V. P. Biju, A. L. Rogach, L. Xiao, S. Jia, *J. Phys. Chem. Lett.* **2018**, *9*, 6934.

[34] S. Seth, T. Ahmed, A. Samanta, *J. Phys. Chem. Lett.* **2018**, *9*, 7007.

[35] Z. Li, G. Zhang, B. Li, R. Chen, C. Qin, Y. Gao, L. Xiao, S. Jia, *Appl. Phys. Lett.* **2017**, *111*, 153106.

**ADVANCED
SCIENCE NEWS**

www.advancedsciencenews.com

**NANO · MICRO
small**

www.small-journal.com

[36] G. Nair, J. Zhao, M. G. Bawendi, *Nano Lett.* **2011**, *11*, 1136.

[37] B. Li, G. Zhang, Y. Zhang, C. Yang, W. Guo, Y. Peng, R. Chen, C. Qin, Y. Gao, J. Hu, R. Wu, J. Ma, H. Zhong, Y. Zheng, L. Xiao, S. Jia, *J. Phys. Chem. Lett.* **2020**, *11*, 10425.

[38] G.-F. Zhang, C.-G. Yang, Y. Ge, Y.-G. Peng, R.-Y. Chen, C.-B. Qin, Y. Gao, L. Zhang, H.-Z. Zhong, Y.-J. Zheng, L.-T. Xiao, S.-T. Jia, *Front. Phys.* **2019**, *14*, 63601.

[39] C. Yang, R. Xiao, S. Zhou, Y. Yang, G. Zhang, B. Li, W. Guo, X. Han, D. Wang, X. Bai, J. Li, R. Chen, C. Qin, J. Hu, L. Feng, L. Xiao, S. Jia, *ACS Photonics* **2021**, *8*, 2538.

[40] Y.-S. Park, W. K. Bae, J. M. Pietryga, V. I. Klimov, *ACS Nano* **2014**, *8*, 7288.

[41] N. S. Makarov, S. Guo, O. Isaienko, W. Liu, I. Robel, V. I. Klimov, *Nano Lett.* **2016**, *16*, 2349.

[42] X. Chen, Y. Lou, A. C. Samia, C. Burda, *Nano Lett.* **2003**, *3*, 799.

[43] B. Huang, H. Yang, L. Zhang, Y. Yuan, Y. Cui, J. Zhang, *Nanoscale* **2018**, *10*, 18331.

[44] H. Yang, L. Zhang, Y. Tang, W. Xiang, X. Wang, M. Xiao, Y. Cui, J. Zhang, *J. Phys. Chem. C* **2021**, *125*, 10759.

[45] B. Li, G. Zhang, Z. Wang, Z. Li, R. Chen, C. Qin, Y. Gao, L. Xiao, S. Jia, *Sci. Rep.* **2016**, *6*, 32662.

[46] F. Gao, P. Bajwa, A. Nguyen, C. D. Heyes, *ACS Nano* **2017**, *11*, 2905.

[47] C. L. Choi, K. J. Koski, S. Sivasankar, A. P. Alivisatos, *Nano Lett.* **2009**, *9*, 3544.

[48] Z. Zhu, G. Ouyang, G. Yang, *J. Appl. Phys.* **2010**, *108*, 083511.

[49] W. K. Bae, L. A. Padilha, Y.-S. Park, H. Mcdaniel, I. Robel, J. M. Pietryga, V. I. Klimov, *ACS Nano* **2013**, *7*, 3411.

[50] X. Hou, Y. Li, H. Qin, X. Peng, *J. Chem. Phys.* **2019**, *151*, 234703.

[51] T. Ahmed, S. Seth, A. Samanta, *ACS Nano* **2019**, *13*, 13537.

[52] J. Kang, L.-W. Wang, *J. Phys. Chem. Lett.* **2017**, *8*, 489.

[53] R. Chen, B. Xia, W. Zhou, G. Zhang, C. Qin, J. Hu, I. G. Scheblykin, L. Xiao, *Adv. Photonics Res.* **2022**, *3*, 2100271.

[54] R. Chen, J. Li, A. Dobrovolsky, S. González Carrero, M. Gerhard, M. E. Messing, V. Chirvony, J. Pérez Prieto, I. G. Scheblykin, *Adv. Opt. Mater.* **2020**, *8*, 1901642.

[55] R. Chen, B. Xia, W. Zhou, W. Guan, G. Zhang, C. Qin, J. Hu, L. Xiao, S. Jia, *Opt. Express* **2021**, *29*, 1851.

[56] M. Gerhard, B. Louis, R. Camacho, A. Merdasa, J. Li, A. Kiligaridis, A. Dobrovolsky, J. Hofkens, I. G. Scheblykin, *Nat. Commun.* **2019**, *10*, 1698.

[57] H. Yuan, E. Debroye, G. Caliandro, K. P. F. Janssen, J. Van Loon, C. E. A. Kirschhock, J. A. Martens, J. Hofkens, M. B. J. Roeffaers, *ACS Omega* **2016**, *1*, 148.

[58] Q. A. Akkerman, G. Rainò, M. V. Kovalenko, L. Manna, *Nat. Mater.* **2018**, *17*, 394.

[59] H. Huang, M. I. Bodnarchuk, S. V. Kershaw, M. V. Kovalenko, A. L. Rogach, *ACS Energy Lett.* **2017**, *2*, 2071.

[60] V. I. Klimov, D. W. Mcbranch, *Phys. Rev. B* **1997**, *55*, 13173.

[61] Y.-S. Park, W. K. Bae, L. A. Padilha, J. M. Pietryga, V. I. Klimov, *Nano Lett.* **2014**, *14*, 396.

[62] C. Zhu, M. Marczak, L. Feld, S. C. Boehme, C. Bernasconi, A. Moskalenko, I. Cherniukh, D. Dirin, M. I. Bodnarchuk, M. V. Kovalenko, G. Rainò, *Nano Lett.* **2022**, *22*, 3751.

[63] J. Cho, Y. K. Jung, J.-K. Lee, *J. Mater. Chem.* **2012**, *22*, 10827.